

# How tropical convection couples high moist static energy over land and ocean

Yi Zhang<sup>1</sup> and Stephan Fueglistaler<sup>1</sup>

<sup>1</sup>Princeton University

October 30, 2023

## Abstract

We show that in the tropics, tropical atmospheric dynamics force the subcloud moist static energy (MSE) over land and ocean to be very similar in, and only in, regions of deep convection. Using observed rainfall as a proxy for convection and reanalysis data to calculate MSE, we show that subcloud MSE in the non-convective regions may differ substantially between land and ocean but is uniform across latitudes in convective regions even on a daily timescale. This result holds also in CMIP5 model simulations of past cold and future warm climates. Furthermore, the distribution of rainfall amount in subcloud MSE is very similar over land and ocean with the peak at 343 J/g and a half width at half maximum of 3 J/g. As a result, the annual-maximum subcloud MSE at each location over land and ocean is subject to a common upper bound set by the convective regions.

1           **How tropical convection couples high moist static**  
2           **energy over land and ocean**

3           **Yi Zhang<sup>1</sup>, Stephan Fueglistaler<sup>1,2</sup>**

4           <sup>1</sup>Program in Atmospheric and Oceanic Sciences, Princeton University, Sayre Hall, Princeton NJ 08544,  
5           USA.

6           <sup>2</sup>Dept. of Geosciences, Princeton University, Guyot Hall, Princeton NJ 08544, USA.

7           **Key Points:**

- 8           • The utility of quasi-equilibrium and weak temperature gradient theories (QE-WTG)  
9           can be demonstrated by a rainfall-weighting method.
- 10          • Observed convection occurs at very similar subcloud moist static energy across  
11          all latitudes in the inner tropics as a result of QE-WTG.
- 12          • The highest moist static energy values are tightly coupled over land and ocean,  
13          while the lower values are free to differ.

**Abstract**

We show that in the tropics, tropical atmospheric dynamics force the subcloud moist static energy (MSE) over land and ocean to be very similar in, and only in, regions of deep convection. Using observed rainfall as a proxy for convection and reanalysis data to calculate MSE, we show that subcloud MSE in the non-convective regions may differ substantially between land and ocean but is uniform across latitudes in convective regions even on a daily timescale. This result holds also in CMIP5 model simulations of past cold and future warm climates. Furthermore, the distribution of rainfall amount in subcloud MSE is very similar over land and ocean with the peak at 343 J/g and a half width at half maximum of 3 J/g. As a result, the annual-maximum subcloud MSE at each location over land and ocean is subject to a common upper bound set by the convective regions.

**Plain Language Summary**

An extremely idealized picture of the tropical atmospheric dynamics is that deep convection sets a horizontally uniform free tropospheric troposphere profile. Here, we show that despite the idealization, this simple picture is very useful in explaining the observations; Convection occurs at very similar spatially uniform subcloud MSE regardless of over land or ocean.

**1 Introduction**

The tropics show, even at equal latitudes and despite a relatively uniform annual mean insolation, a large variety of local climates ranging from regions with highest rainfall globally to deserts. Given the paramount importance of rainfall over land for ecosystems and humans, the processes governing its distribution and how it may change in the future are focus of intense efforts both in terms of improved process representations in numerical climate models, and development of theories to interpret observations and model results (e.g., Lintner & Chiang, 2005; Seneviratne et al., 2013; Pendergrass et al., 2017; Byrne & O’Gorman, 2015). Understanding climate over land inevitably requires understanding its connection to the oceans. A fundamental difference between land and ocean is that over land, evapotranspiration is constrained by available moisture and, as a consequence, sensible heat flux plays a larger role over land than ocean. An important corol-

44 lary of this surface energy budget consideration that is robustly observed in global cli-  
45 mate model simulations is that the surface temperature response to radiative forcing is  
46 larger over land than ocean (Manabe et al., 1991).

47 The limited evaporation over land not only affects the partitioning between sen-  
48 sible and latent heat flux, but also leads to different temperature lapse rates in the lower  
49 layers of the troposphere over land and ocean. Joshi et al. (2008) note that in model cal-  
50 culations there exists a level sufficiently high up in the troposphere where temperature  
51 change in response to forcing is similar over land and ocean, and the larger surface tem-  
52 perature response over land then is consistent with the different changes in lapse rates  
53 over land and ocean. Byrne and O’Gorman (2013a) formulate this effect in terms of the  
54 equality of equivalent potential temperature averaged over land and ocean as a result  
55 of weak temperature gradients in the free troposphere and convective quasi-equilibrium,  
56 which is largely supported by simulations with idealized climate models. However, they  
57 also notice that this equality breaks down in realistic climate models (Byrne & O’Gorman,  
58 2013b), and the changes in the mean surface equivalent potential temperature, rather  
59 than the mean equivalent potential temperatures themselves, are more similar over land  
60 and ocean (Byrne & O’Gorman, 2013b; Byrne & O’Gorman, 2018).

61 In the following, we present observation and model results to provide a more pre-  
62 cise picture how tropical atmospheric dynamics couple the moist static static (MSE; equiv-  
63 alent to the equivalent potential temperature used in (Byrne & O’Gorman, 2013a, 2013b))  
64 of air near the surface over land and ocean to the free atmosphere. We show that the  
65 subcloud MSE where convection occurs is roughly constant with latitude in the inner  
66 tropics (about 20°S-20°N) and very similar over land and ocean, which may not be ex-  
67 pected in light of the well-documented land-ocean contrast of tropical convection (Robinson  
68 et al., 2011; Matsui et al., 2016). Notably, this similarity holds across all latitudes of the  
69 inner tropics even on a daily timescale. As a result, the connection in subcloud MSE over  
70 land and ocean is only established in the highest MSE values that compose the convective  
71 regions.

## 2 Data and Method

### 2.1 Subcloud MSE

Subcloud MSE is computed using ERA-Interim 6-hourly reanalysis data on  $0.75^\circ \times 0.75^\circ$  grid and pressure levels (Dee et al., 2011). Moist static energy  $h$  is calculated following the definition

$$h = c_p T + gz + Lq, \quad (1)$$

where  $c_p$  is the heat capacity of air,  $T$  is temperature,  $g$  is gravitational acceleration,  $z$  is height,  $L$  is the latent heat of water, and  $q$  is the mixing ratio of water vapor. Standard values used in climate models and reanalysis data are adopted here, namely  $c_p = 1005 \text{ J/kg}$ ,  $L = 2.5 \times 10^6 \text{ J/kg}$  and  $g = 9.8 \text{ m/s}^2$ . The subcloud layer is the portion of the boundary layer extending from the surface to the average altitude of the base of clouds (American Meteorological Society, 2012). Here, we calculate the lifting condensation level on 6-hourly time frequency. Subcloud MSE is then the average MSE either within the layer between the ground and the LCL when the LCL is within the boundary layer, or within the boundary layer when the LCL is higher than the boundary-layer top (no-cloud case). The 6-hourly subcloud MSE is averaged to a daily timescale to match the time resolution of the rainfall observation.

### 2.2 Convective subcloud MSE

The convective (subcloud) MSE is calculated by weighting the subcloud MSE in each grid box with the corresponding rainfall received, i.e., rainfall intensity multiplied by the area of the grid box, following the rainfall-weighting method in Flannaghan et al. (2014); Fueglistaler et al. (2015):

$$\text{Convective subcloud MSE} = \frac{\sum_i P_i h_i}{\sum_i P_i} \quad (2)$$

Daily rainfall observations from Tropical Rainfall Measuring Mission (TRMM) (Huffman et al., 2007) from 2001 to 2014 of  $0.25^\circ \times 0.25^\circ$  resolution are interpolated to the ERA-Interim grid conserving total precipitation fluxes. The convective (subcloud) MSE can be loosely interpreted as the subcloud MSE weighted by the mass flux transported from the subcloud layer to the free atmosphere by deep convection, as convective mass flux scales roughly linearly with rainfall (Raymond et al., 2015). The resolution of the data used here (order 100 km) does not allow distinguishing between convective rain (1-10 km)

100 and stratiform rain ( $\sim 100$  km) (Houze, 1997), which may introduce some ambiguity in  
 101 the determination of convective MSE. For the convective MSE as a function of latitude,  
 102 the subcloud MSE in each latitude band is first calculated on a yearly basis before av-  
 103 eraged over the chosen period and hence is not influenced by trends or interannual vari-  
 104 ability in total tropical rainfall.

### 105 **3 Results**

#### 106 **3.1 The MSE threshold for convection – A zeroth-order picture**

107 The tropical atmosphere can be seen as consisting of a boundary layer with diverse  
 108 temperature, humidity, and topography (the three components of MSE) and a free tro-  
 109 posphere that is comparatively homogenous. Deep convection transports boundary layer  
 110 air upward into the free atmosphere. Once the free atmosphere is filled with buoyant air  
 111 originating from the warm and humid boundary layer, it suppresses upward motion in  
 112 the colder regions, establishing a threshold for convection. More quantitatively, the con-  
 113 straint from atmospheric dynamics can be expressed as a combination of convective quasi-  
 114 equilibrium (QE) and weak temperature gradient (WTG) (Byrne & O’Gorman, 2013a),  
 115 subsequently referred to as QE-WTG. Strict quasi-equilibrium assumes that convection  
 116 maintains the subcloud MSE equal to the saturated MSE aloft in the free atmosphere  
 117 (e.g., Arakawa & Schubert, 1974; Emanuel, 2007) (The saturated MSE only strongly de-  
 118 pends on the air temperature). Weak temperature gradient states that the free atmo-  
 119 sphere cannot sustain substantial horizontal temperature gradients due to the smallness  
 120 of the Coriolis parameter in the tropics (e.g., Charney, 1963; A. H. Sobel & Bretherton,  
 121 2000). Consequently, at the limit of strict quasi-equilibrium and zero temperature gra-  
 122 dient, simultaneously convecting regions, regardless of over land or ocean, should have  
 123 the same subcloud MSE which we refer to as the MSE threshold for convection. While  
 124 previous studies (Byrne & O’Gorman, 2013a, 2013b; Byrne & O’Gorman, 2018) eval-  
 125 uate the QE-WTG picture with the large-scale mean MSE over land and ocean, we ar-  
 126 gue that QE-WTG should be evaluated only in the regions where deep convection cou-  
 127 ples the MSE in the subcloud layer to the free atmosphere and does not apply to the re-  
 128 gions where the subcloud MSE is too low to reach the threshold for convection. Lever-  
 129 aging the aforementioned rainfall-weighting method, we are able show that QE-WTG  
 130 apply to each latitude in the observations, even on a daily timescale, and there is a clear  
 131 breakdown of the theoretical picture around  $20^\circ$  in both hemispheres.

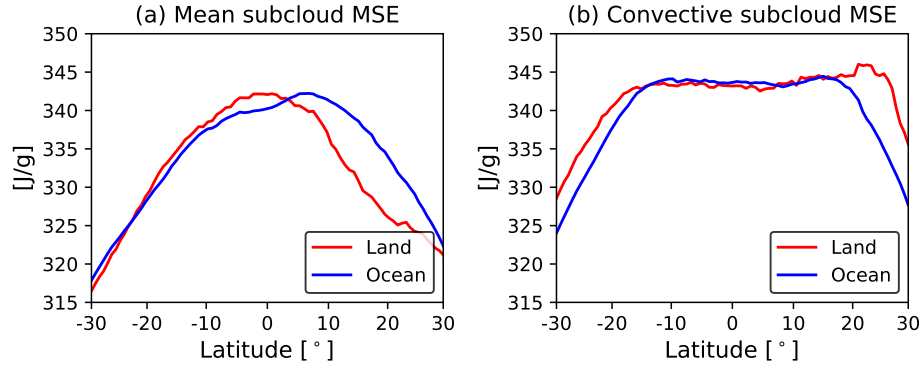


**Figure 1.** Zonal-mean (a) and convective (b) subcloud moist static energy (MSE) over land (red) and ocean (blue). Subcloud MSE is derived from ERA-Interim and rainfall is from TRMM. Daily data from 2001 to 2014 are used. The convective subcloud MSE is determined by weighting the subcloud MSE at each longitude with the corresponding rainfall within each latitudinal band of  $0.75^\circ$  wide.

132 The zonal-mean subcloud MSE (Fig. 1(a)) peaks around the equator reflecting the  
 133 annual-mean solar forcing, whereas the convective subcloud MSE (Fig. 1(b)) is roughly  
 134 uniform throughout the inner tropics and very similar between land and ocean, reflect-  
 135 ing the weak horizontal temperature gradients in the free atmosphere. The sharp drop-  
 136 off at about  $20^\circ$  in both hemispheres indicates where the Coriolis effect is no longer neg-  
 137 ligible and QE-WTG breaks down. As a result, rainfall in the subtropics can occur ei-  
 138 ther at very low subcloud MSE when induced by the extratropical eddies (Funatsu &  
 139 Waugh, 2008) or at very high subcloud MSE during the South Asian monsoon which cre-  
 140 ates the peak in the convective MSE around  $25^\circ\text{N}$  over land (Boos & Kuang, 2010). The  
 141 contrast between the mean and the convective subcloud MSE resolves the aforementioned  
 142 inconsistency between the strict QE-WTG theory and the realistic simulations mentioned  
 143 in (Byrne & O’Gorman, 2013b); Convection only occurs in the part of the domain where  
 144 the subcloud MSE is high enough to reach the tropically uniform MSE threshold of about  
 145  $343\text{ J/g}$  shown in Fig. 1(b), and in the part of the domain that is not convecting sub-  
 146 cloud MSE is not coupled to the free atmosphere and therefore can differ between  
 147 land and ocean.

148 A more stringent test examines how effectively QE-WTG works on a daily basis.  
 149 Fig. 2 shows the seasonal evolution of the zonal-mean subcloud MSE in the convective

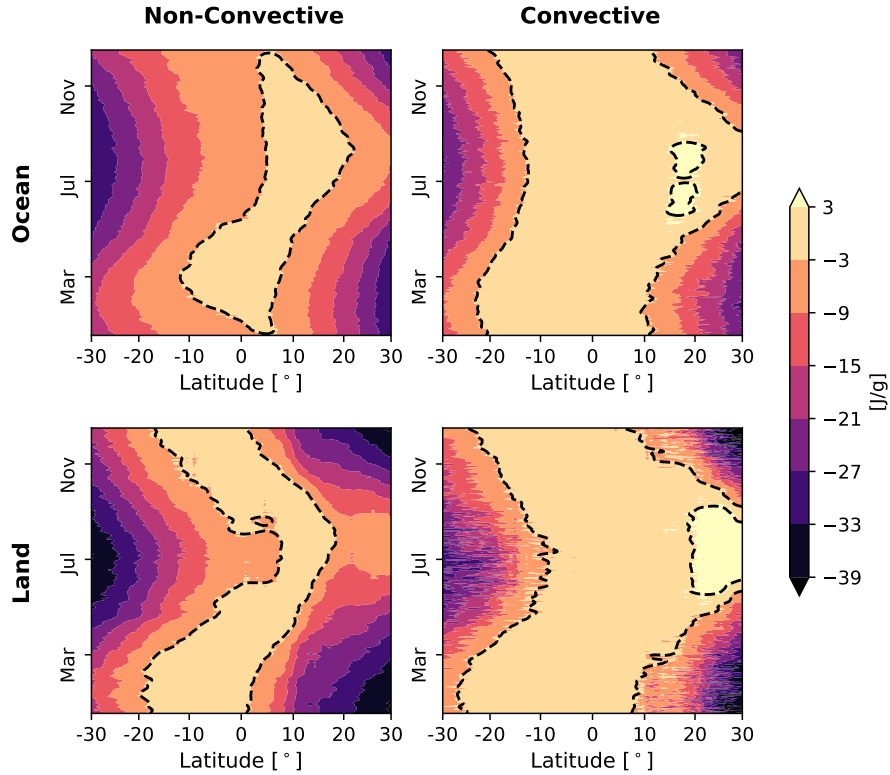


**Figure 2.** The mean subcloud moist static energy (MSE) as a function of latitude and day of year in the non-convective and convective regions over ocean and land. Daily data are used from ERA-Interim and TRMM between 2001 and 2014. Convective and non-convective regions are identified with a rainfall threshold of 6 mm/day. The dashed contour lines indicate the subcloud MSE within  $\pm 3$  J/g relative to a common reference value (see text).

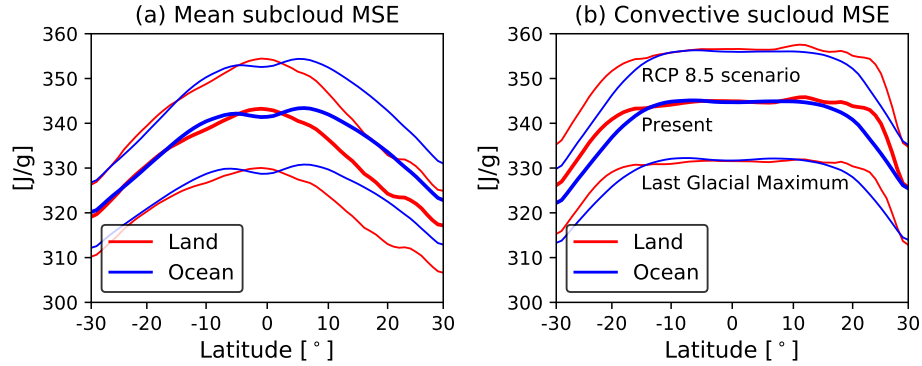


**Figure 3.** Zonal-mean (a) and convective (b) subcloud moist static energy (MSE) for model simulations. The multi-model mean of monthly data from CMIP5 models (See Table S1) are shown. Three experiments are shown from bottom to top: the Last Glacial Maximum, the period from 1979 to 2005 in the simulation of current climate (labeled “Present”), and the last 20 years of the 21st century in the global warming simulation (labeled “RCP 8.5 scenario”).

150 regions (left column) and non-convective regions (right column) over land (lower row)  
 151 and ocean (upper row). Here the convective MSE is defined as the mean subcloud MSE  
 152 where the rain rate is above 6 mm/day (A. Sobel et al., 2002) and *vice versa* for the non-  
 153 convective MSE. The results are not sensitive to the choice of a rainfall threshold from  
 154 2 mm/day to 20 mm/day (Figs. S1, S2). This method is different from the rainfall-weighting  
 155 method used in Fig. 1 but yields similar convective MSE values, essentially because rain-  
 156 fall anywhere in the inner tropics occurs at very similar subcloud MSE. To facilitate the  
 157 comparison, a reference value for each day of year, calculated as the mean subcloud MSE  
 158 in the convective regions over equatorial ( $5^{\circ}\text{S}$ - $5^{\circ}\text{N}$ ) ocean, is subtracted. Even on a sin-  
 159 gle day of year, the convective MSE is still uniform over a broad range in latitude, though  
 160 this latitudinal range has seasonality (Fig. 2, right column). The seasonal evolution of  
 161 the non-convective MSE has more prominent land-ocean contrast than the convective  
 162 MSE (indicated by the shapes of the dashed black contours), supporting the concept that  
 163 only the subcloud MSE in the convective regions over land and ocean are tied to the uni-  
 164 form temperature in the free atmosphere.

165 The physics involved in the QE-WTG mechanism does not rely on the mean cli-  
 166 matic state, therefore QE-WTG is expected to hold in all climates. Global climate mod-  
 167 els from the Coupled Model Intercomparison Project phase 5 (CMIP5) (Taylor et al.,

168 2012) that correctly reproduce the observed uniform convective MSE in the simulations  
 169 of the present climate (Fig. S3 and Table S1) also show a uniform convective MSE in  
 170 the projections of a much warmer climate under the Representative Concentration Path-  
 171 way 8.5 (RCP8.5) emission scenario (Fig. 3). Model simulations of the much colder Last  
 172 Glacial Maximum also show a uniform convective MSE over both land and ocean. There-  
 173 fore, Fig. 3 demonstrates the validity of QE-WTG in a wide range of climates.

### 174 **3.2 Finite width of the MSE threshold for convection – A first-order cor-** 175 **rection**

176 The latitudinal uniformity of the convective subcloud MSE in the inner tropics and  
 177 its similarity between land and ocean (Fig. 1, 2) provide observational support for the  
 178 zeroth-order picture. However, it is well established that factors such as the mid-tropospheric  
 179 humidity (Emanuel, 2019; Brown & Zhang, 1997), convective inhibition (Mapes, 2000),  
 180 low-level convergence (Lindzen & Nigam, 1987; Back & Bretherton, 2009), and station-  
 181 ary or transient equatorial waves (Gill, 1980; Kiladis et al., 2009) all affect the trigger-  
 182 ing of convection. How can these complicating factors be reconciled with the simple pic-  
 183 ture of a uniform MSE threshold for convection?

184 The convective MSE threshold shown in Fig. 1(b) is a weighted mean over a range  
 185 of subcloud MSE values rather than a single MSE value. Fig. 4(a) shows the total amount  
 186 of rainfall that falls into each subcloud MSE bin of a width of  $0.2 \text{ J/g}$ . This rainfall dis-  
 187 tribution can be roughly regarded as the convective mass flux distribution as a function  
 188 of subcloud MSE. If QE-WTG were strict, this distribution would be a Dirac function  
 189 at the highest subcloud MSE. In the observed climate, however, the majority of rainfall  
 190 occurs around  $343 \text{ J/g}$ —the value is comparable to the convective MSE (Fig. 1(a))—with  
 191 a Half Width at Half Maximum (HWHM) of  $3 \text{ J/g}$ . The half width of  $3 \text{ J/g}$  then encaps-  
 192 ulates the previously mentioned factors that affect the local triggering of convection.  
 193 This width is narrow compared to the entire range of the tropical subcloud MSE of about  
 194  $60 \text{ J/g}$ . Remarkably, the shape of the rainfall distribution as a function of subcloud MSE  
 195 is also similar between land and ocean, a result not predicted by the theoretical limit of  
 196 QE-WTG.

197 The tails of the rainfall distribution at very high subcloud MSE above  $350 \text{ J/g}$  and  
 198 low subcloud MSE below  $336 \text{ J/g}$  are somewhat different for land and ocean, due to the

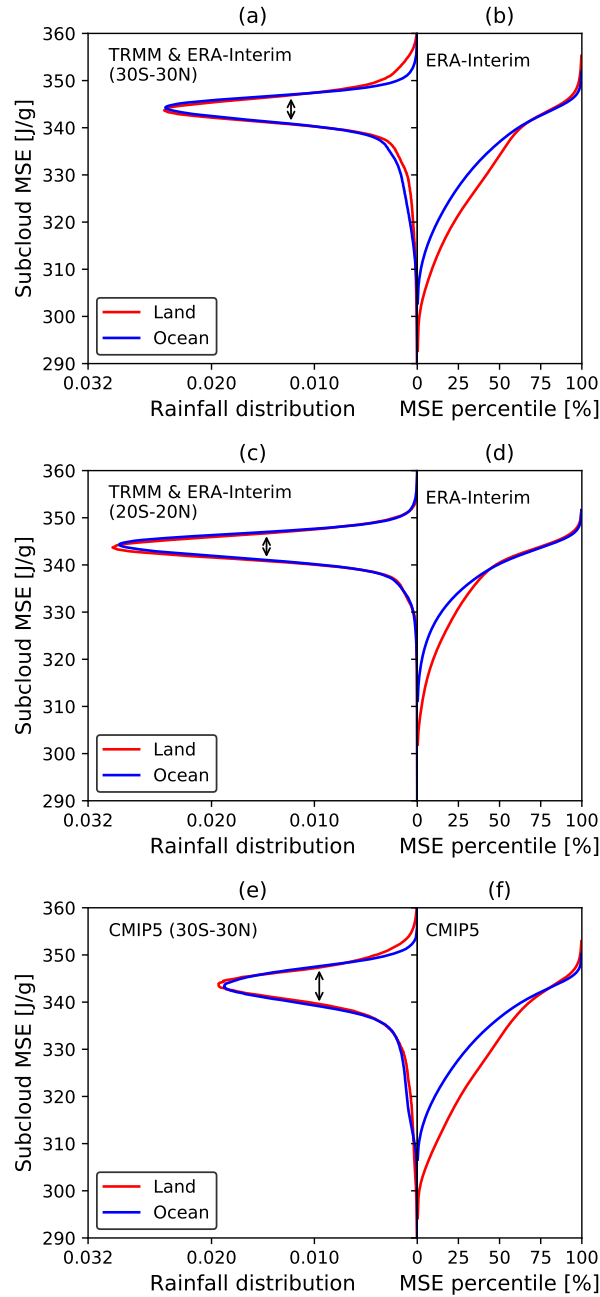


**Figure 4.** Rainfall distribution as a function of subcloud MSE (left panels) and the corresponding percentiles of subcloud MSE (right panels). (a) and (b) show rainfall from TRMM and subcloud MSE from ERA-Interim between  $30^{\circ}\text{S}$  and  $30^{\circ}\text{N}$ . (c) and (d) are the same as (a) and (b) but with data between  $20^{\circ}\text{S}$  and  $20^{\circ}\text{N}$ . (e) and (f) are the same as (a) and (b) but is the multi-model mean of monthly output from CMIP5 models in the coupled simulation from 1979 to 2005 (Table S1). The double arrows indicate where the HWHM is evaluated.

199 break-down of QE-WTG in the subtropics. When the latitudinal range is restricted to  
 200 20°S-20°N (Fig. 4(c)), the tails disappear and a convective mode centered at 343 J/g emerges  
 201 which is almost identical over land and ocean.

202 Fig. 4(e) is the same as Fig. 4(a) but for the CMIP5 multi-model mean. The width  
 203 of the MSE threshold is wider than that in the observations, because it is an average of  
 204 models with slightly different mean states. In fact, the half width for an individual CMIP5  
 205 model is also 3 J/g on average.

206 To put the magnitude of the width into context, we compare it with typical MSE  
 207 changes due to departure from the strict QE-WTG: Observed convective available po-  
 208 tential energy (CAPE) varies between 0 and 4 J/g (Williams & Renno, 1993; Gettelman  
 209 et al., 2002) and the free tropospheric temperature varies by order 1 K horizontally (e.g.  
 210 Fueglistaler et al., 2009) which translates to about 2 J/g of subcloud MSE. It is thus not  
 211 obvious which factor contributes more given the similar amplitudes. We also notice that  
 212 the width is not strongly dependent on the time frequency (daily or monthly) of data.

213 Figs. 4(b,d,f) show the corresponding percentiles of subcloud MSE sorted in ascend-  
 214 ing order and averaged in equal-area bins. Fig. 4(b) reiterates that only the highest sub-  
 215 cloud MSE values between 30°S and 30°N are coupled over land and ocean while the low  
 216 subcloud MSE values are free to differ – the upper 30% of subcloud MSE has almost iden-  
 217 tical distribution over land and ocean while the lower 70% of the subcloud MSE over ocean  
 218 is systematically higher than that over land. In addition, Figs. 4(b,d) highlight an in-  
 219 teresting aspect of the Earth’s tropical climate: The convective area fraction is approx-  
 220 imately equal over land and ocean.

## 221 4 Conclusion and outlook

222 We show that a simple theoretical picture of the tropical atmosphere based on the  
 223 convective quasi-equilibrium and the weak-temperature-gradient assumptions (QE-WTG)  
 224 can effectively explain the observations. In accordance with QE-WTG, the convective  
 225 subcloud MSE is roughly constant with latitude between 20°S and 20°N on a daily timescale  
 226 in the observed current climate and in the simulated past and future climates. The util-  
 227 ity of QE-WTG is manifested in its capability of reconciling the land-ocean contrast. The  
 228 vastly different land and ocean surfaces share almost identical convective subcloud MSE,  
 229 distribution of highest subcloud MSE values, and precipitation distribution as a func-

230 tion of subcloud MSE. Whereas the role of subcloud MSE forcing the free troposphere  
231 has been well appreciated in tropical convection, we demonstrate that the horizontally  
232 uniform free tropospheric temperature forces the highest subcloud MSE values to be sim-  
233 ilar over land and ocean, which is an interesting aspect of convection in the tropics. These  
234 results fill the gap between the idealized, conceptual understanding of the tropical at-  
235 mospheric dynamics and the real world consisting of diverse regional climates.

236 An important implication of our results is that the maximum subcloud MSE at a  
237 given location, either over land or over ocean, is subject to a common upper bound set  
238 by the convective regions. As moist static energy is related to heat stress metrics (Fischer  
239 & Knutti, 2013; Sherwood & Huber, 2010; Byrne & O’Gorman, 2013b) and as is pointed  
240 out in Byrne and O’Gorman (2013b) that the mean heat stress over land is controlled  
241 by the ocean, our results suggest that atmospheric dynamics may also control heat stress  
242 extremes in the tropics.

## 243 **Acknowledgments**

244 We thank Isaac Held and Nadir Jeevanjee for thoughtful feedback and discussion, and  
245 Julius Busecke and Allison Hogikyan for suggestions on an earlier version of the manuscript.  
246 Y.Z. acknowledges support from the Cooperative Institute for Modeling the Earth Sys-  
247 tem (CIMES). S.F. acknowledges support from National Science Foundation Awards AGS-  
248 1417659 and AGS-1743753. We acknowledge the European Centre for Medium-range Weather  
249 Forecast (ECMWF) for providing ERA-Interim data ([https://www.ecmwf.int/en/forecasts/  
250 datasets/archive-datasets/reanalysisdatasets/era-interim](https://www.ecmwf.int/en/forecasts/datasets/archive-datasets/reanalysisdatasets/era-interim)). We acknowledge  
251 the National Aeronautics and Space Administration (NASA) for providing Tropical Rain-  
252 fall Measuring Mission (TRMM) 3B42 data ([https://disc.gsfc.nasa.gov/datasets/  
253 TRMM\\_3B42RT\\_Daily\\_V7/summary](https://disc.gsfc.nasa.gov/datasets/TRMM_3B42RT_Daily_V7/summary)). We acknowledge the World Climate Research Pro-  
254 gramme’s Working Group on Coupled Modelling and climate modeling groups (Table  
255 S1) for producing CMIP5 model data (<https://esgf-node.llnl.gov/projects/cmip5>).

## 256 **References**

- 257 American Meteorological Society. (2012). *Subcloud layer, glossary of meteorology*.  
258 ([http://glossary.ametsoc.org/wiki/Subcloud\\_layer](http://glossary.ametsoc.org/wiki/Subcloud_layer), Last accessed on  
259 2019-11-2)
- 260 Arakawa, A., & Schubert, W. H. (1974). Interaction of a cumulus cloud ensemble

- 261 with the large-scale environment, part i. *J. Atmos. Sci.*, *31*(3), 674–701.
- 262 Back, L., & Bretherton, C. (2009). On the relationship between sst gradients,  
263 boundary layer winds, and convergence over the tropical oceans. *J. Climate*,  
264 *22*, 4182–4196. doi: 10.1175/2009JCLI2392.1
- 265 Boos, W., & Kuang, Z. (2010). Dominant control of the south asian monsoon by  
266 orographic insulation versus plateau heating. *Nature*, *463*, 218–222.
- 267 Brown, R. G., & Zhang, C. (1997). Variability of midtropospheric moisture and  
268 its effect on cloud-top height distribution during toga coare. *J. Atmos. Sci.*,  
269 *54*(23), 2760–2774.
- 270 Byrne, M. P., & O’Gorman, P. A. (2013a). Land–ocean warming contrast over  
271 a wide range of climates: Convective quasi-equilibrium theory and idealized  
272 simulations. *Journal of Climate*, *26*(12), 4000–4016.
- 273 Byrne, M. P., & O’Gorman, P. A. (2013b). Link between land-ocean warming  
274 contrast and surface relative humidities in simulations with coupled climate  
275 models. *Geophysical Research Letters*, *40*(19), 5223–5227.
- 276 Byrne, M. P., & O’Gorman, P. A. (2015). The response of precipitation minus evap-  
277 otranspiration to climate warming: Why the “wet-get-wetter, dry-get-drier”  
278 scaling does not hold over land. *Journal of Climate*, *28*(20), 8078–8092.
- 279 Byrne, M. P., & O’Gorman, P. A. (2018). Trends in continental temperature  
280 and humidity directly linked to ocean warming. *Proceedings of the National*  
281 *Academy of Sciences*, *115*(19), 4863–4868.
- 282 Charney, J. (1963). A note on large-scale motions in the tropics. *J. Atmos. Sci.*, *20*,  
283 607–609.
- 284 Dee, D. P., Uppala, S., Simmons, A., Berrisford, P., Poli, P., Kobayashi, S., . . . oth-  
285 ers (2011). The era-interim reanalysis: Configuration and performance of the  
286 data assimilation system. *Quarterly Journal of the royal meteorological society*,  
287 *137*(656), 553–597.
- 288 Emanuel, K. (2007). Quasi-equilibrium dynamics of the tropical atmosphere. *The*  
289 *Global Circulation of the Atmosphere*, 186–218.
- 290 Emanuel, K. (2019). Inferences from simple models of slow, convectively coupled  
291 processes. *J. Atmos. Sci.*, *76*(1), 195–208.
- 292 Fischer, E. M., & Knutti, R. (2013). Robust projections of combined humidity and  
293 temperature extremes. *Nature Climate Change*, *3*(2), 126.

- 294 Flannaghan, T. J., Fueglistaler, S., Held, I. M., Po-Chedley, S., Wyman, B., & Zhao,  
 295 M. (2014). Tropical temperature trends in Atmospheric General Circulation  
 296 Model simulations and the impact of uncertainties in observed SSTs. *J.*  
 297 *Geophys. Res.*, *119*(23), 13,327–13,337. doi: 10.1002/2014JD022365
- 298 Fueglistaler, S., Dessler, A. E., Dunkerton, T. J., Folkins, I., Fu, Q., & Mote,  
 299 P. W. (2009). Tropical tropopause layer. *Rev. Geophys.*, *47*, RG1004. doi:  
 300 10.1029/2008RG000267
- 301 Fueglistaler, S., Radley, C., & Held, I. M. (2015). The distribution of precipita-  
 302 tion and the spread in tropical upper tropospheric temperature trends. *Geo-*  
 303 *phys. Res. Letts.*, *42*(14), 6000-6007. doi: 10.1002/2015GL064966
- 304 Funatsu, B., & Waugh, D. (2008). Connections between potential vorticity intru-  
 305 sions and convection in the eastern tropical pacific. *J. Atmos. Sci.*, *65*, 987–  
 306 1002. doi: 10.1175/2007JAS2248.1
- 307 Gettelman, A., Seidel, D., Wheeler, M., & Ross, R. (2002). Multidecadal trends  
 308 in tropical convective available potential energy. *J. Geophys. Res. Atmos.*,  
 309 *107*(D21).
- 310 Gill, A. E. (1980). Some simple solutions for heat-induced tropical circulation. *Q. J.*  
 311 *Roy. Meteor. Soc.*, *106*(449), 447–462.
- 312 Houze, R. (1997). Stratiform precipitation in regions of convection: A meteorological  
 313 paradox? *Bulletin American Meteorological Society*, *78*(10), 2179–2196.
- 314 Huffman, G. J., Bolvin, D. T., Nelkin, E. J., Wolff, D. B., Adler, R. F., Gu, G., ...  
 315 Stocker, E. F. (2007). The trmm multisatellite precipitation analysis (tmpa):  
 316 Quasi-global, multiyear, combined-sensor precipitation estimates at fine scales.  
 317 *Journal of hydrometeorology*, *8*(1), 38–55.
- 318 Joshi, M. M., Gregory, J. M., Webb, M. J., Sexton, D. M. H., & Johns, T. C.  
 319 (2008). Mechanisms for the land/sea warming contrast exhibited by simu-  
 320 lations of climate change. *Clim. Dynamics*, *30*, 455-465.
- 321 Kiladis, G. N., Wheeler, M., Haertel, P., Straub, K., & Roundy, P. (2009). Convec-  
 322 tively coupled equatorial waves. *Rev. Geophys.*, *47*, RG2003. doi: 10.1029/  
 323 2008RG000266
- 324 Lindzen, R., & Nigam, S. (1987). On the role of sea surface temperature gradients in  
 325 forcing low-level winds and convergence in the tropics. *J. Atmos. Sci.*, *44*(17),  
 326 2418–2436.

- 327 Lintner, B. R., & Chiang, J. C. (2005). Reorganization of tropical climate during  
328 el nino: A weak temperature gradient approach. *Journal of climate*, *18*(24),  
329 5312–5329.
- 330 Manabe, S., Stouffer, R., Spelman, M., & Bryan, K. (1991). Transient responses of a  
331 coupled ocean–atmosphere model to gradual changes of atmospheric co2. part  
332 i: Annual mean response. *J. Clim.*, *4*, 785–818.
- 333 Mapes, B. E. (2000). Convective inhibition, subgrid-scale triggering energy, and  
334 stratiform instability in a toy tropical wave model. *J. Atmos. Sci.*, *57*(10),  
335 1515–1535.
- 336 Matsui, T., Chern, J.-D., Tao, W.-K., Lang, S., Satoh, M., Hashino, T., & Kubota,  
337 T. (2016). On the land–ocean contrast of tropical convection and micro-  
338 physics statistics derived from trmm satellite signals and global storm-resolving  
339 models. *Journal of Hydrometeorology*, *17*(5), 1425–1445.
- 340 Pendergrass, A. G., Knutti, R., Lehner, F., Deser, C., & Sanderson, B. M. (2017).  
341 Precipitation variability increases in a warmer climate. *Scientific reports*, *7*(1),  
342 17966.
- 343 Raymond, D., Fuchs, Z., Gjorgjievska, S., & Sessions, S. (2015). Balanced dynamics  
344 and convection in the tropical troposphere. *J. Adv. Model Earth Sys.*, *7*, 1093-  
345 1116. doi: 10.1002/2015MS000467
- 346 Robinson, F., Sherwood, S., Gerstle, D., Liu, C., & Kirshbaum, D. J. (2011). Ex-  
347 ploring the land–ocean contrast in convective vigor using islands. *Journal of*  
348 *the Atmospheric Sciences*, *68*(3), 602–618.
- 349 Seneviratne, S. I., Wilhelm, M., Stanelle, T., van den Hurk, B., Hagemann, S., Berg,  
350 A., . . . others (2013). Impact of soil moisture-climate feedbacks on cmip5 pro-  
351 jections: First results from the glace-cmip5 experiment. *Geophysical Research*  
352 *Letters*, *40*(19), 5212–5217.
- 353 Sherwood, S. C., & Huber, M. (2010). An adaptability limit to climate change  
354 due to heat stress. *Proceedings of the National Academy of Sciences*, *107*(21),  
355 9552–9555.
- 356 Sobel, A., Held, I., & Bretherton, C. (2002). The ENSO Signal in Tropical Tropo-  
357 spheric Temperature. *J. Climate*, *15*(18), 2702-2706.
- 358 Sobel, A. H., & Bretherton, C. S. (2000). Modeling tropical precipitation in a single  
359 column. *J. Climate*, *13*(24), 4378–4392.

- 360 Taylor, K. E., Stouffer, R. J., & Meehl, G. A. (2012). An overview of cmip5 and the  
361 experiment design. *Bull. Am. Meteorol. Soc.*, *93*(4), 485–498.
- 362 Williams, E., & Renno, N. (1993). An analysis of the conditional instability of the  
363 tropical atmosphere. *Monthly Weather Review*, *121*(1), 21–36.

# Supporting Information for “How tropical convection couples high moist static energy over land and ocean”

Yi Zhang<sup>1</sup>, Stephan Fueglistaler<sup>1,2</sup>

<sup>1</sup>Program in Atmospheric and Oceanic Sciences, Princeton University, Sayre Hall, Princeton NJ 08544, USA.

<sup>2</sup>Dept. of Geosciences, Princeton University, Guyot Hall, Princeton NJ 08544, USA.

## Contents of this file

1. Text S1 to S2
2. Figures S1 to S3
3. Table S1

### Text S1. Land mask

Coastal regions and islands are known to have substantial amounts of rainfall. The horizontal resolution of data used in this work implies ambiguity regarding the separation into land and ocean which could damp the differences between the calculated convective MSE over land and ocean. We therefore employ a strict criterion to eliminate the grid boxes that are not overwhelmingly land or ocean. A grid box is classified as ocean if the land area fraction is less than 5%, and is classified as land if the land area fraction is more than 95%. The remaining “coastal” grid cells taking up about 5% of area of the

---

entire tropics are discarded in this analysis. For ERA-Interim, the land cover type data (MCD12C1) on  $0.05^\circ \times 0.05^\circ$  grid from Moderate Resolution Imaging Spectroradiometer data (Friedl & Sulla-Menashe, 2015) is used to calculate the fraction of land in each box of the reanalysis grid. For CMIP5 models, the land area fraction provided by the modeling centers is used.

**Text S2.** Convective subcloud moist static energy (MSE) in CMIP5 models.

A simplified procedure for the calculation of the subcloud MSE is used for the CMIP5 model output where less detailed boundary layer information is available. The reduced vertical resolution of the CMIP5 model output to the standard pressure levels (1000, 925, 850 hPa ...) precludes the same accuracy as with the reanalysis data in the determination of the lifting condensation level (LCL). In addition, most models do not extrapolate data over land to the 1000 hPa level. We thus use a simplified procedure to estimate the subcloud MSE in the CMIP5 models: We use the 925 hPa as the generic upper boundary of the subcloud layer following Williams, Pierrehumbert, and Huber (2009); Williams and Pierrehumbert (2017). For models that report all the required data on the near-surface level (temperature, specific humidity, orography) and the 925 hPa pressure level (temperature, specific humidity, geopotential height), subcloud MSE is the average of the near-surface MSE and the 925-hPa MSE; For models that do not report all the required data on the near-surface level but report extrapolated information on the 1000 hPa over land, subcloud MSE is the average of the MSE on 1000 and 925 hPa pressure levels. This calculation is based on monthly mean data. To estimate the error introduced by the simplification, we apply this simplified procedure to the monthly mean ERA-Interim

and TRMM data and find that the convective MSE is still similar over land and ocean on monthly timescale.

Fig. S3 shows the convective MSE over land vs. over ocean calculated with the simplified calculation for the CMIP5 models. Most models produce very similar convective subcloud MSE over land and ocean, but there are a few strong outliers. The multi-model mean values shown in Figs. 3 and 4 only include those models (SI Appendix, Table S1) that reasonably reproduce the observation in the Historical experiment and have a difference in the convective subcloud MSE between land and ocean of less than 2 J/g. For the multi-model mean, all the zonal-mean quantities are first calculated on the models' native grids and then interpolated onto a common 1° meridional grid.

## References

- Friedl, M., & Sulla-Menashe, D. (2015). *Mcd12c1 modis/terra+ aqua land cover type yearly l3 global 0.05deg cmg v006 [data set]* (Vol. 10). doi: <https://doi.org/10.5067/MODIS/MCD12C1.006>
- Williams, I. N., & Pierrehumbert, R. T. (2017). Observational evidence against strongly stabilizing tropical cloud feedbacks. *Geophysical Research Letters*, *44*(3), 1503–1510.
- Williams, I. N., Pierrehumbert, R. T., & Huber, M. (2009). Global warming, convective threshold and false thermostats. *Geophysical Research Letters*, *36*(21).

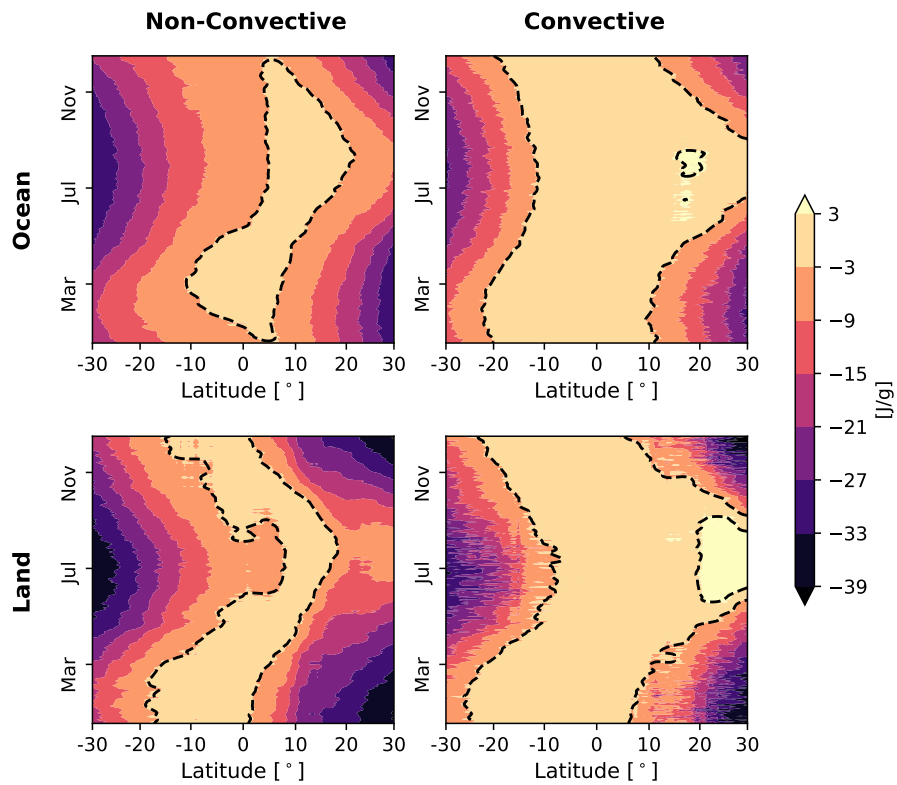


**Figure S1.** The mean subcloud moist static energy (MSE) as a function of latitude and day of year in the non-convective and convective regions over land and ocean. Convective and non-convective regions are identified with a rainfall threshold of 2 mm/day.

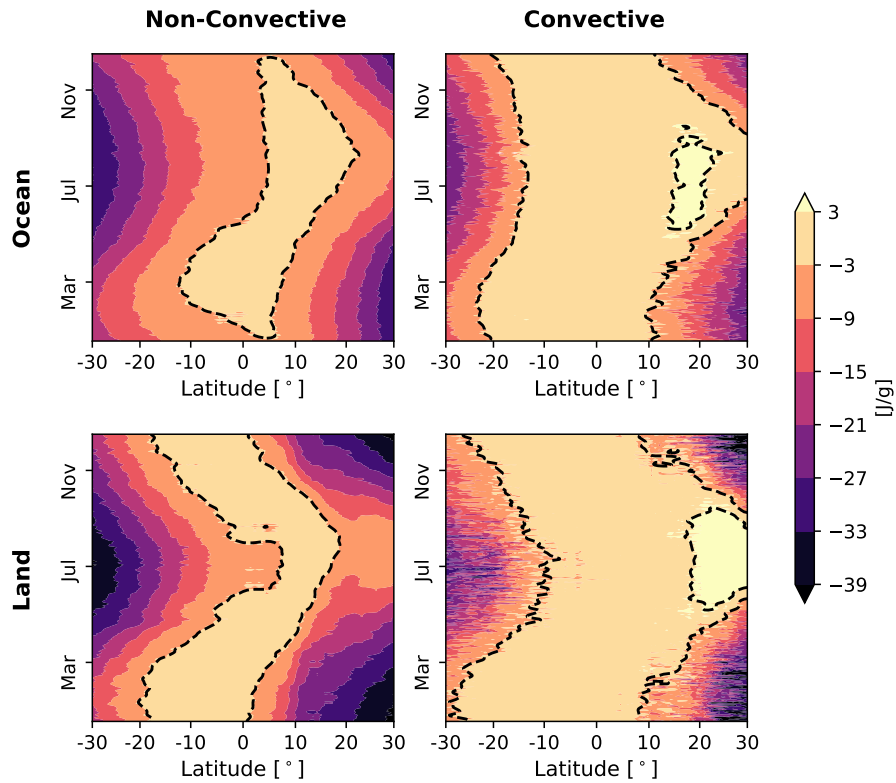


**Figure S2.** The mean subcloud moist static energy (MSE) as a function of latitude and day of year in the non-convective and convective regions over land and ocean. Convective and non-convective regions are identified with a rainfall threshold of 20 mm/day.

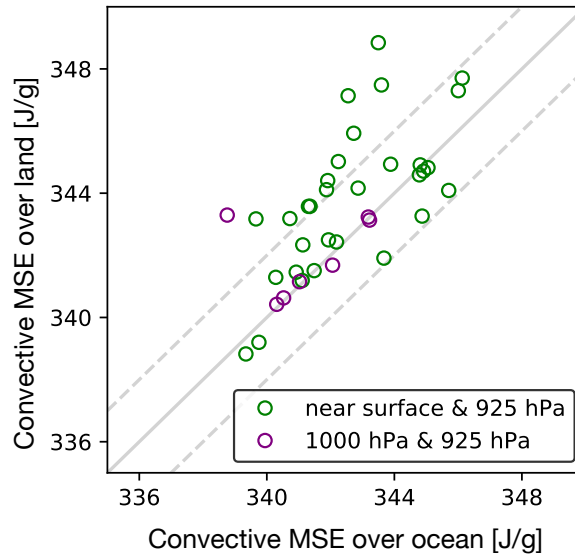


**Figure S3.** Convective subcloud MSE over land and ocean for CMIP5 models during the period from year 1979 to 2005 in the Historical experiment. Green circles are models where atmospheric near-surface data are available and subcloud MSE is calculated with the near-surface and the 925hPa level data. Purple circles are models that do not report complete near-surface data but report data over land at 1000 hPa and subcloud MSE is calculated with the 1000 hPa level and 925 hPa level data. The multi-model means shown includes only models that approximately reproduce the observation and have less than 2 J/g difference (dashed lines) between land and ocean (Table S1).

**Table S1.** Table of CMIP5 models used. ✓ and ✗ indicates whether a model is shown or not, while blank indicates a model that does not report complete information (See Text S2). “S” or “L” indicates the subcloud MSE is calculated with near-surface data or 1000 hPa data (See Text S2).

Model Name	Method	Historical	RCP 8.5	LGM	Institute ID
ACCESS1-0	S	✗	✗		CSIRO-BOM
ACCESS1-3	S	✗	✗		CSIRO-BOM
BCC-CSM1.1	S	✓	✓		BCC
CCSM4	S	✓	✓	✓	NCAR
CESM1-BGC	S	✓	✓		NSF-DOE-NCAR
CESM1-CAM5	S	✓	✓		NSF-DOE-NCAR
CESM1-FASTCHEM	S	✓			NSF-DOE-NCAR
CESM1-WACCM	S	✓			NSF-DOE-NCAR
CMCC-CESM	L	✓	✓		CMCC
CMCC-CM	L	✓	✓		CMCC
CMCC-CMS	L	✓	✓		CMCC
CNRM-CM5	S	✓	✓	✓	CNRM-CERFACS
CNRM-CM5-2	S	✓			CNRM-CERFACS
CSIRO-Mk3-6-0	S	✓	✓		CSIRO-QCCCE
CanESM2	S	✓	✓		CCCMA
GFDL-CM3	S	✓	✓		NOAA GFDL
GFDL-ESM2G	S	✗	✗		NOAA GFDL
GFDL-ESM2M	S	✗	✗		NOAA GFDL
GISS-E2-H	S	✗	✗		NASA GISS
GISS-E2-R	S	✗	✗		NASA GISS
HadGEM2-AO	S	✓	✓		NIMR/KMA
HadGEM2-CC	S	✓	✓		MOHC
HadGEM2-ES	S	✓	✓		MOHC
INM-CM4	L	✗			INM
IPSL-CM5A-LR	S	✗	✗	✓	IPSL
IPSL-CM5A-MR	S	✗	✗		IPSL
IPSL-CM5B-LR	S	✓	✓		IPSL
MIROC-ESM	S	✗	✗	✓	MIROC
MIROC-ESM-CHEM	S	✗	✗		MIROC
MIROC4h	S	✓			MIROC
MIROC5	S	✗	✗		MIROC
MPI-ESM-LR	L	✓	✓		MPI-M
MPI-ESM-MR	L	✓	✓		MPI-M
MPI-ESM-P	L	✓		✓	MPI-M
MRI-CGCM3	S	✓	✓	✓	MRI
MRI-ESM1	S	✓	✓		MRI
NorESM1-M	S	✓	✓		NCC
NorESM1-ME	S	✓			NCC